Chemical Science

ROYAL SOCIETY OF CHEMISTRY

EDGE ARTICLE

View Article Online
View Journal | View Issue

Cite this: *Chem. Sci.*, 2023, **14**, 1138

All publication charges for this article have been paid for by the Royal Society of Chemistry

Received 22nd November 2022
Accepted 26th December 2022

DOI: 10.1039/d2sc06436g

rsc.li/chemical-science

Regulating the assembly and expansion of the silver cluster from the Ag_{37} to Ag_{46} nanowheel driven by heteroanions†

Rakesh Kumar Gupta, [a] Li Li,[a] Zhi Wang, [a] Bao-Liang Han, [a] Lei Feng,[a] Zhi-Yong Gao, [b] Chen-Ho Tung [a] and Di Sun *[a]

Precise control over the shape and size of metal nanoclusters through anion template-driven self-assembly is one of the key scientific goals in the nanocluster community, however, it is still not understood comprehensively. In this work, we report the controllable synthesis and atomically precise structures of silver nanowheels **Ag37** and **Ag46**, using homo (Cl^- ions) and heteroanion (Cl^- and CrO_4^{2-} ions) template strategies, along with macrocyclic *p*-phenyl-thiacalix[4]arene and small $^iPrS^-$ ligands. Structural analyses revealed that in **Ag37**, Cl^- ions serve as both local and global templates, whereas CrO_4^{2-} ions function as local and Cl^- ions as global templates in **Ag46**, resulting in a pentagonal nanowheel (**Ag37**) and a hexagonal (**Ag46**) nanowheel. The larger ionic size and more negative charges of CrO_4^{2-} ions than Cl^- ions offer more coordination sites for the silver atoms and are believed to be the key factors that drive the nanowheel core to expand significantly. Also, by taking advantage of the deep cavity of thiacalix[4]arene with an extended phenyl group, **Ag46** has been used as a host material for dye adsorption depending on the charge and size of organic dyes. The successful use of heteroanions to control the expansion of well-defined silver nanowheels fills the knowledge gap in understanding the directing role of heteroanions in dictating the shape and size of nanoclusters at the atomic level.

Introduction

Metal nanoclusters (NCs) are highly attractive synthetic targets in cluster chemistry due to their potential application as catalysts, sensors, and bioimaging agents, to name a few.[1] Synthesizing NCs in a controlled manner is much more challenging than the trial-and-error approach because such processes always involve the intricate assembly of multiple components controlled by thermodynamic and kinetic factors.[2] Furthermore, controlled synthesis offers the functionalization of novel metal NCs with customizable properties and applications that are unavailable to simpler systems.

After decades of effort, the anion-template method is well-established for the synthesis of silver NCs. It has been proven to be useful for adding complexity and functionality with a high probability of creating high-nuclearity NCs that are somewhat predictable.[3] As a subclass, heteroanion templates with different sizes, geometries, and charge states have received less attention in the synthesis of silver NCs than homoanion templates.[4] Xie *et al.* used Cl^- and $[(O)_2V_2O_6]^{4-}$ ions to produce an Ag_{36} NC.[5] Our group isolated a high-nuclearity $[(SO_4)_2(W_5O_{19})_2@Ag_{90}]$ NC, where the heteroanions of SO_4^{2-} and $W_5O_{19}^{8-}$ are both *in situ* generated.[6] We are motivated to use the concept of assembling heteroanion templates in the early stage of the assembly, which may interfere with the formation of the core by aggregating silver atoms around them in different ways and thus is a feasible way to regulate the shape, size, and specific metal atom and ligand arrangement of silver NCs. A comparative study of template effects (homo and heteroanion templates) on the structure and figuring out the factors that lead to the core variation of the NCs and their structural details are really complex processes and are rarely investigated.

On the other hand, protecting ligands are also crucial for controlling the physicochemical properties, core size, and structural stability of silver NCs.[7] Besides using common thiolate,[8] phosphine,[9] and alkynyl ligands,[10] or combinations of these,[11] the unusual macrocyclic ligands (*e.g.*, thiacalix[4]arene) hold promising potential for passivating silver NCs, such as Ag_{18},[12] Ag_{21},[13] Ag_{34},[14] Ag_{35},[15] Ag_{42},[16] Ag_{88},[17] and Ag_{155}.[18] In addition, thiacalix[4]arene or its derivative represents a fascinating cavity that could be potentially used to encapsulate

[a]*Key Laboratory of Colloid and Interface Chemistry, Ministry of Education, School of Chemistry and Chemical Engineering, State Key Laboratory of Crystal Materials, Shandong University, Ji'nan 250100, China. E-mail: dsun@sdu.edu.cn*

[b]*School of Chemistry and Chemical Engineering, Henan Normal University, Xinxiang, 453007, China*

† Electronic supplementary information (ESI) available: Synthesis details, IR, UV-vis, and PXRD data, details of the data collection and structure refinements, and crystal data. CCDC 2206151 and 2206152 for **Ag46** and **Ag37**. For ESI and crystallographic data in CIF or other electronic format see DOI: https://doi.org/10.1039/d2sc06436g

guest molecules.[19] As such, it would be of great interest to further develop silver NCs protected by thiacalix[4]arene, especially those comprising different anion templates, which will give us an opportunity to better understand the controlled synthesis, assembly, and structural evolution mechanism.

Here, we present two silver nanowheels $[Cl_7@Ag_{37}Na(PTC4A)_5(^iPrS)_{10}(DMF)_4(CH_3CN)_2]\cdot Cl\cdot 2CH_2Cl_2$ (**Ag37**) and $[(CrO_4)_2Cl_6@Ag_{46}(PTC4A)_6(^iPrS)_{12}(CH_3CN)_6]$ (**Ag46**) that manifest the core size expansion relying on the heteroanion template strategy in the presence of macrocyclic *p*-phenylthiacalix[4]arene (H_4PTC4A) as a protecting ligand. More specifically, with the Cl^- ions, an Ag_{37} NC is obtained, exhibiting a pentagonal waterwheel-like entity, while with a heteroanion combination (Cl^- and CrO_4^{2-}), the metal core expands from Ag_{37} to Ag_{46}, adopting a hexagonal waterwheel-like entity. Furthermore, the facile and scalable synthesis of **Ag46** has been demonstrated for the selective adsorption and separation of cationic dyes methylene blue (MB) and rhodamine B (RhB) in water through host–guest interactions in the extended cavity of the $PTC4A^{4-}$ ligand. To the best of our knowledge, this is the first example of atomically precise silver NCs being used for dye adsorption studies. These observations will inspire the use of heteroanion templates to design NC assemblies with various geometries and functional properties.

Results and discussion

Under the solvothermal conditions, the reaction of polymeric $[^iPrSAg]_n$, PhCOOAg, H_4PTC4A, and NaCl as a chloride source produced yellow fusiform crystals of **Ag37** in a 5% yield (1.3 mg; based on H_4PTC4A), whereas NaCl and $(NH_4)_2Cr_2O_7$ (sources of Cl^- and CrO_4^{2-}, respectively) produced black-red cubic crystals of **Ag46** in a 50% yield (14 mg; based on H_4PTC4A) (Scheme 1 and Fig. S1†). Of note, from the perspective of scientific research, the feasibility of scale-up synthesis is important for property exploration and large-scale applications.[20] However, metal NCs are known to be sensitive to synthesis conditions, and it is extremely difficult to achieve high-yield synthesis. Fortunately, we managed to achieve a tenfold scale-up for the synthesis of **Ag46**, which produced 140 mg of the final product from a one pot reaction. The synthetic details and a series of characterization studies, including single-crystal X-ray diffraction (SCXRD), powder X-ray diffraction (PXRD), UV-vis spectroscopy, and infrared (IR) spectroscopy, are provided in the ESI.†

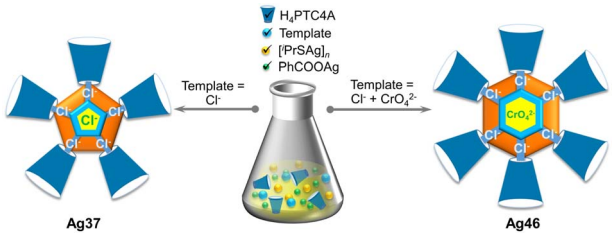

Scheme 1 Synthetic routes for **Ag37** and **Ag46**.

X-ray structures of Ag37 and Ag46

SCXRD analyses reveal that **Ag37** crystallizes in the triclinic system with the space group of $P\bar{1}$, whereas **Ag46** crystallizes in the monoclinic $P2_1/n$ space group (Table S1†). The asymmetric units of both the nanowheels comprise an entire molecule. As shown in Fig. 1, **Ag37** possesses a waterwheel-like structure with a pentagonal metal core that is 1.3 nm × 0.4 nm (excluding the organic ligands). The structure of **Ag37** is composed of 37 Ag^+ cations and 1 Na^+ cation, 7 Cl^- templates, 5 $PTC4A^{4-}$ and 10 $^iPrS^-$ ligands, and coordinated solvent molecules of 2 CH_3CN and 4 DMF (Fig. 1a and b). The metallic skeleton of 37 silver atoms is a Ag_2 (core)@Ag_{35} (shell) configuration, which can be described as three parts: in the centre, two silver atoms act as the innermost core, and on the surface, two eclipsed Ag_5 pentagons above and below the equatorial plane and a bracelet-like Ag_{25} ring form the Ag_{35} shell (Fig. S2†). The Ag···Ag distances fall in the range of 2.76–3.37 Å. The Ag_{35} shell is covered by external organic ligands and solvent molecules. All the $PTC4A^{4-}$ ligands are deprotonated and adopt a distorted cone conformation, coordinating with five Ag atoms using a μ_5-κ_O^3:κ_O^3:κ_O^3:κ_O^3:κ_S^1:κ_S^1:κ_S^1:κ_S^1 mode to produce a shuttlecock-like Ag_5@PTC4A unit (Fig. 1c). Among the Ag_5@PTC4A units, four Ag atoms are symmetrically arranged, each of which is

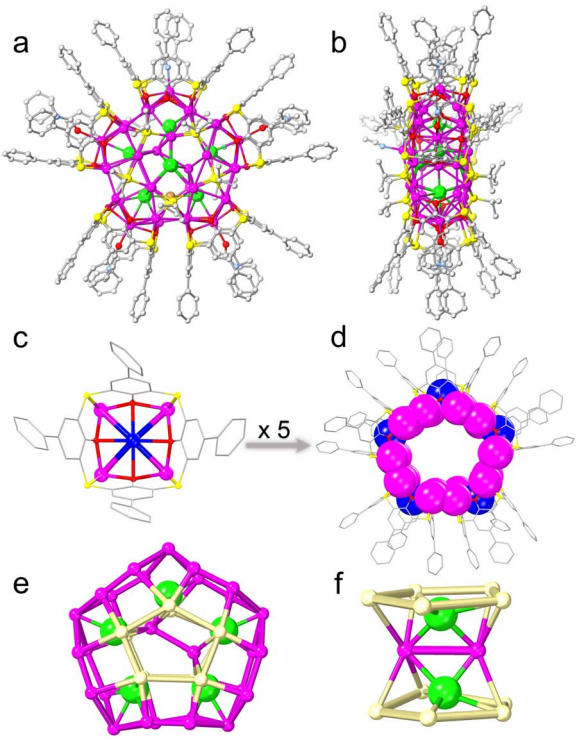

Fig. 1 (a) and (b) Total X-ray crystal structure of **Ag37** viewed along two orthogonal directions. (c) Coordination mode of the $PTC4A^{4-}$ ligand towards Ag atoms. (d) The pentagonal arrangement of $PTC4A^{4-}$ ligands on the Ag_{25} bracelet. The silver atoms are shown in a space-filling pattern. (e) Five Cl^- ions held between the Ag_2 core and the Ag_{35} shell. (f) The other two Cl^- ions capping on the inner Ag_2 core. Colour code: Ag, purple, blue, and pale yellow; Na, brown; O, red; S, yellow; Cl, green; C, gray; N, pale blue.

ligated by two phenolic O atoms and one bridging S atom. There is one more Ag atom at the centre of the pentagonal metal core (Fig. 1c; blue ball), approximately 1.4–1.7 Å offset above the center of the Ag_4 quadrangle formed by four silver atoms at the bottom, connected by four phenolic O atoms, and is further stabilized by either DMF or CH_3CN (Fig. S3†). The units are interconnected with each other by argentophilic interactions to form bracelet-like Ag_{25}@$(PTC4A)_5$ (Fig. 1d). The Ag–O and Ag–S bonds linked to $PTC4A^{4-}$ ligands are within the limits of 2.23–2.63 Å and 2.52–2.63 Å, respectively. All the $^{i}PrS^{-}$ ligands are distributed uniformly on both sides of the nanowheel, connecting the Ag_{25}@$(PTC4A)_5$ unit and two Ag_5 pentagons above and below the equatorial plane in μ_4-κ^1:κ^1:κ^1:κ^1 mode (Ag–S distances, 2.35–2.54 Å; Fig. S4†).

It is worth mentioning that each Ag_5@PTC4A unit is subsequently connected with a Cl^- template, which fills the inner space of the silver shell around the Ag_2 core in a pentagonal distribution (Fig. 1e). Two Ag_5 pentagons on the surface of the silver shell are arranged in a face-to-face manner above and below the Cl^- ion layer. These five Cl^- ions (2 μ_5 and 3 μ_4) play a critical role in the global template effect of connecting the outer Ag_{35} shell and the inner Ag_2 core. Interestingly, the other two Cl^- ions are enclosed in the center of the silver shell, covering the Ag_2 core at both ends, up and down. These two Cl^- ions exert the local template effect to ligate to the innermost two Ag atoms and three Ag atoms of the Ag_5 pentagon in the same μ_5 mode (Fig. 1f). **Ag37** has a wavy ABAB pattern along the [100] direction, and one of the phenyl groups of the $PTC4A^{4-}$ ligand penetrates into the cavity of the $PTC4A^{4-}$ ligand of the nanowheel in the adjacent layer (Fig. S5†).

On the other hand, **Ag46** is a hexagonal waterwheel-like structure with an enlarged radial diameter of 1.70 nm and nearly the same axial thickness of 0.4 nm as that of **Ag37**. In detail, the structure has a fascinating hexagonal core–shell skeleton with an inner Ag_4 core in the center with up to six Cl^- and two CrO_4^{2-} as anion templates, enveloped by a larger Ag_{42} shell, which is further covered and stabilized by 12 $^{i}PrS^{-}$ and 6 $PTCTA^{4-}$ ligands together with 6 CH_3CN solvent molecules (Fig. 2a). Unlike **Ag37**, the outer shell of **Ag46** is anchored by six $PTC4A^{4-}$ ligands, adopting two different coordination modes to form the $[Ag_5@(PTC4A)]_6$ unit: two μ_5-κ_O^3:κ_O^3:κ_O^3:κ_S^1:κ_S^1:κ_S^1 and four μ_5-κ_O^3:κ_O^3:κ_O^2:κ_O^2:κ_S^1:κ_S^1:κ_S^1. And each of the central Ag atoms (Fig. 2b; blue balls) in the bowl of Ag_5@(PTC4A) units is ligated to one CH_3CN molecule (Fig. S6†). Six such units are linked together by argentophilic interactions to form larger bracelet-like Ag_{30}@$(PTC4A)_6$ with a hexagonal arrangement (Fig. 2b). The $^{i}PrS^{-}$ ligands link Ag_{30}@$(PTC4A)_6$ and two Ag_6 hexagons above and below the equatorial plane through sulfur atoms, adopting μ_4-κ^1:κ^1:κ^1:κ^1 ligation mode (Fig. S7†). Within this structure, six Cl^- ions (1 μ_3, 2 μ_4, 2 μ_6, and 1 μ_7) act as global templates and are arranged in a hexagonal ring that connects the outer Ag_{42} shell and the innermost Ag_4 core, providing reasonable stability to the entire nanowheel (Fig. 2c). In addition, the two middle Ag_6 hexagons on the surface of the silver shell and the innermost Ag_4 tetragon are interiorly supported by two CrO_4^{2-} ions *via* μ_8-κ^3:κ^3:κ^1:κ^1 and μ_8-κ^4:κ^2:κ^1:κ^1 modes (Fig. 2d and e).

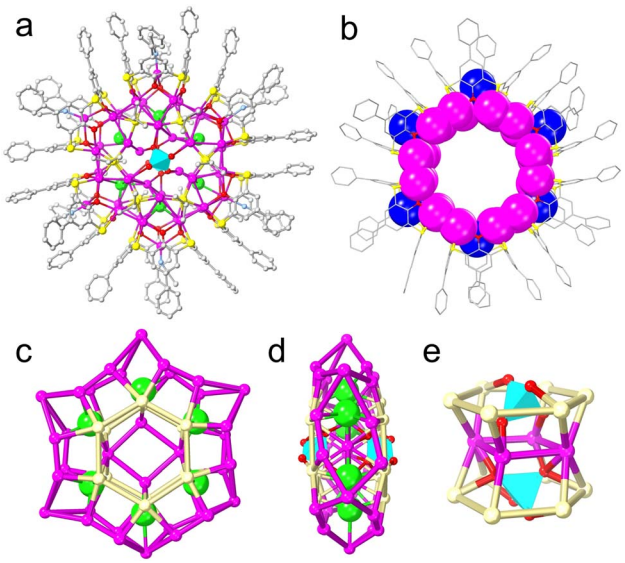

Fig. 2 (a) Total X-ray crystal structure of **Ag46**. (b) The hexagonal arrangement of $PTC4A^{4-}$ ligands on the Ag_{30} bracelet. The silver atoms are shown in a space-filling pattern. (c) Six Cl^- ions anchored between the Ag_4 core and the Ag_{42} shell. (d) The structure of $Ag_4@(CrO_4)_2Cl_6@Ag_{42}$. (e) Two CrO_4^{2-} anions capping on the inner Ag_4 core. The cyan polyhedra represent CrO_4^{2-}. Colour code: Ag, purple, blue, and pale yellow; O, red; S, yellow; Cl, green; C, gray; N, pale blue.

Crystal packing of **Ag46** shows a layered structure along the [010] direction, and the nanowheels in each layer are horizontally arranged side by side (Fig. S8†).

The most intriguing aspects of **Ag37** and **Ag46** are the central Cl^- and CrO_4^{2-} templates. In the case of **Ag37**, two singly charged Cl^- ions as local anion templates passivated a linear Ag_2 core in the center. And another set of five Cl^- ions with a pentagonal distribution serves as a global template in the interior. Not only that, the number of silver atoms in each part of the outer shell (2 Ag_5 pentagons above and below the equatorial plane and 1 Ag_{25} bracelet) and ligands (5 $PTC4A^{4-}$ and 10 $^{i}PrS^{-}$) is either 5 or a multiple of 5, which makes the configuration of the overall structure appear to be a pentagonal arrangement. However, in **Ag46**, the larger CrO_4^{2-} with two negative charges acts as a local anion template, giving rise to the larger Ag_4 core. Meanwhile, the number of Cl^- ions (serving as a global template interiorly), silver atoms (two Ag_6 hexagons above and below the equatorial plane and another Ag_{30} bracelet) or the ligands (six $PTC4A^{4-}$ and twelve $^{i}PrS^{-}$) on the outer shell correspondingly enlarged from 5 or a multiple of 5 (in **Ag37**) to 6 or a multiple of 6, resulting in the expansion of the silver nanowheel structure into a hexagonal arrangement. The enclosed CrO_4^{2-} provides more coordination sites, increases the metal coordination tendency, and is supposed to be the critical feature that allows the nanowheel core to expand significantly.

ESI-MS studies of Ag37 and Ag46

Apart from crystallographic data, electrospray ionization mass spectrometry (ESI-MS) is an alternative characterization method

reaching atomic accuracy, which has been widely used to study the solution behavior of metal NCs.[21] We characterized **Ag37** and **Ag46** with a Bruker impact II high definition mass spectrometer using CH_3OH/CH_2Cl_2 as the solvent. As shown in Fig. 3, the most prominent signal containing eight peaks was observed only in the positive mode for **Ag37**, while three peaks were observed in the negative mode for **Ag46** in the m/z range of 3000–12000. The signals at m/z = 4383.535 (**1b**), 4412.498 (**1d**), 4441.486 (**1f**), and 4470.961 (**1h**) correspond to $[NaCl_7@Ag_{37}(PTC4A)_5(^iPrS)_x(H_2O)(OH)_y]^{2+}$ ($x = 6 \sim 9$, $y = 3 \sim 0$; calcd. m/z = 4383.434, 4412.446, 4441.458, and 4470.970), which represents an exchange between $^iPrS^-$ and OH^-. The observed isotopic distribution patterns align with the simulated ones (inset of Fig. 3a). Among them, the species **1h** corresponds well with the parent ion peak of **Ag37** with the loss of one $^iPrS^-$ ligand followed by adding one H_2O. The remaining peaks were assigned as a series of 36-nuclei silver species due to slight coordination disassociation. The summary of the formulae of the assigned peaks is detailed in Table S2.† Discriminatively, the ESI-MS of **Ag46** consists of three predominant peaks carrying two negative charges (**2a–2c**) as shown in Fig. 3b. After identification, we found that all three peaks belonged to the 44-nuclei silver species but with the loss of the CrO_4^{2-} anion (Table S3†). This may be due to the fact that the bulky CrO_4^{2-} is not completely encapsulated in the silver shell and is easily lost after dissolution or during electrospray. These results indicate that **Ag37** and **Ag46** show a slight dissociation of the surface ligand and Ag atom in solution, but both maintain the basic integrity of the skeleton.

Dye adsorption performance of Ag46

The problem of water pollution, initiated by the long-term use of dyes, has become a severe threat to human health. Therefore, the efficient removal of dyes from effluents is critical and urgent.[22] Adsorption is considered to be one of the most promising methods due to its low cost and high efficiency.[23] Because of their hydrophobic and π-electron-rich cavities, calixarenes have recently been introduced as the backbones for constructing metallic and non-metallic containers, successfully inducing these compounds to recognize various guest molecules, such as organic dyes and iodine, as excellent absorbents.[24] Studies suggest that the small size of the cavity in calixarenes makes it hard for dyes to bind. On the other hand, calixarene derivatives with extended aromatic groups could bind dyes more efficiently because of the bigger cavity size and also the possibility of π···π interactions between aromatic groups and dyes.[19,25] From the crystal structures, it is clear that the $PTC4A^{4-}$ ligands adopt a cone conformation and possess a deeper cavity defined by the phenyl group on the upper rim. The average distance between the opposite phenyl groups is 14.7 and 9.9 Å, respectively, and the depth of the cavity is 7.4 Å (Fig. S9 and Table S4†). These cavities are large enough to accommodate suitable guest molecules for inclusion. We envisioned that the $PTC4A^{4-}$-supported silver NC could fully exert the host–guest interaction of the $PTC4A^{4-}$ ligands on its

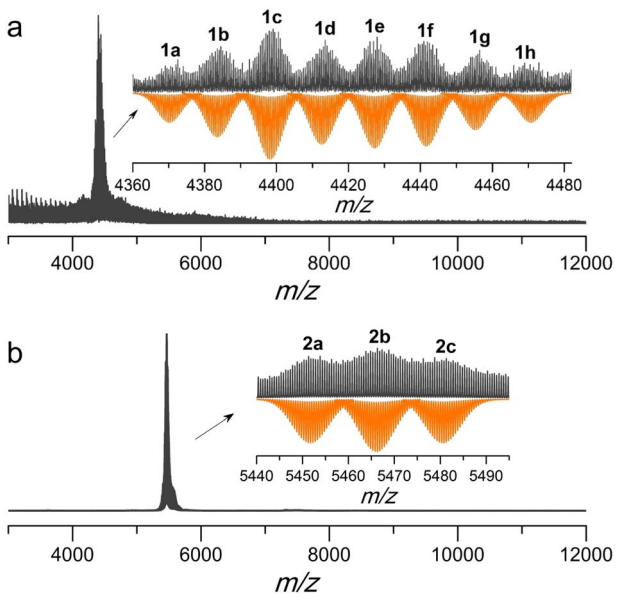

Fig. 3 (a) Positive-ion mode ESI-MS of **Ag37** and (b) negative-ion mode ESI-MS of **Ag46**. Insets: zoom-in experimental (black line) and simulated (orange line) isotope patterns of each labeled species.

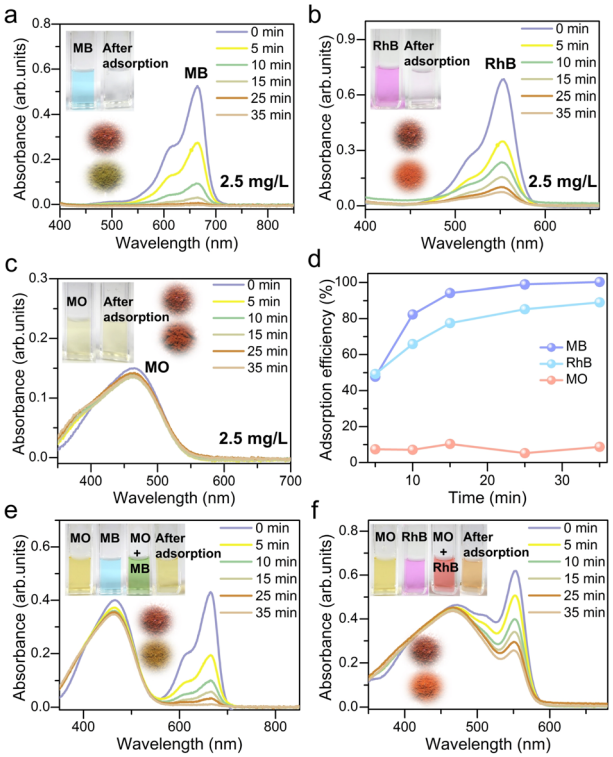

Fig. 4 Temporal evolution of UV-vis absorption spectra of (a) MB, (b) RhB, and (c) MO. (d) The adsorption efficiency of MB, RhB, and MO at the same concentrations. (e) Temporal evolution of UV-vis absorption spectra of MO/MB (concentration ratio of MO and MB = 3 : 1; the concentration of MO = 2.5 mg L^{-1}) and (f) MO/RhB (concentration ratio of MO and RhB = 3 : 1; the concentration of RhB = 2.5 mg L^{-1}). The inset shows the color changes of the aqueous dye solutions and the crystals of **Ag46** before (top) and after adsorption (bottom), respectively.

surface with foreign organic dye molecules. Then, **Ag46** is subjected to dye adsorption studies because of its high synthetic yield (50%, at the gram level) and more free interacting sites on the surface available for dye adsorption.

In order to evaluate the adsorption performance of **Ag46**, three typical organic dyes with different charges and sizes were chosen for measurement at room temperature in the dark: methyl orange (MO), methylene blue (MB), and rhodamine B (RhB) (Table S4†). Among them, both MB and RhB are positively charged, but the size of RhB is larger; MB and MO are similar in size, but MO is negatively charged. Time-dependent UV/vis spectra were collected after adding the freshly prepared crystals of **Ag46** (15 mg) to aqueous solutions of MB, RhB, and MO (2.5 mg L^{-1}), respectively (Fig. 4a–c). As evidenced by the changes in the characteristic absorption maximum of the dye aqueous solutions, only the cationic dyes were absorbed by **Ag46**. This phenomenon was possibly attributed to the electrostatic interaction between the positively charged dyes and the electronegative inner wall of thiacalix[4]arene-based coordination containers (Fig. S10†). Here, the adsorption efficiency for each dye was calculated based on the change in the UV/vis absorbance intensity (100% for MB; 89% for RhB; and 7% for MO within 35 min) (Fig. 4d). Based on selective adsorption of dyes with different charges, **Ag46** may have the potential to separate them in bicomponent solutions. Then, the samples of **Ag46** were added to the mixed dyes MO/MB, respectively. Obviously, only the absorbance (λ_{max}) of MB centered at 665 nm gradually disappeared, indicating that almost all MB was absorbed from the aqueous solution, with the solution colors varying from green to yellow and the sample of **Ag46** changing from brownish red to green-yellow (Fig. 4e). A similar phenomenon was observed, with RhB being selectively separated from the MO/RhB mixture (Fig. 4f).

The results indicate that **Ag46** has highly selective adsorption and separation efficiency for the cationic dyes (MB and RhB) from aqueous solution through the host–guest interaction of the surface cavity, which also inspired us to use **Ag46** as the stationary phase of a chromatographic column. MB, RhB, mixed solutions of MO/MB, and MO/RhB were injected into the chromatographic column, respectively. As shown in Fig. 5, MB and RhB are quickly adsorbed onto **Ag46**, while MO is transported through the column. This successfully separated two kinds of dyes, which could be easily seen with the naked eye (Fig. 5c and d). The above experiments suggest that **Ag46** can serve as a column-chromatographic filter for the separation of dyes and provide a basis for further research on the adsorption performance of thiacalix[4]arene-supported silver NCs.

Molecular docking was conducted to understand and identify the interaction sites between **Ag46** and the dyes (Fig. S11 and S12).† These studies support our hypothesis of the inclusion of dye molecules in the cavity of thiacalix[4]arene *via* noncovalent interactions. **Ag46** binds primarily through π···π interactions with the MB dye (Fig. 6a and Table S5†), whereas RhB shows π···π and C-H_{alkyl}···π interactions (Fig. 6b and Table S5†). To the best of our knowledge, this is the first report of metal NCs being utilized for dye-adsorption and exhibiting excellent selectivity for cationic dyes in water.

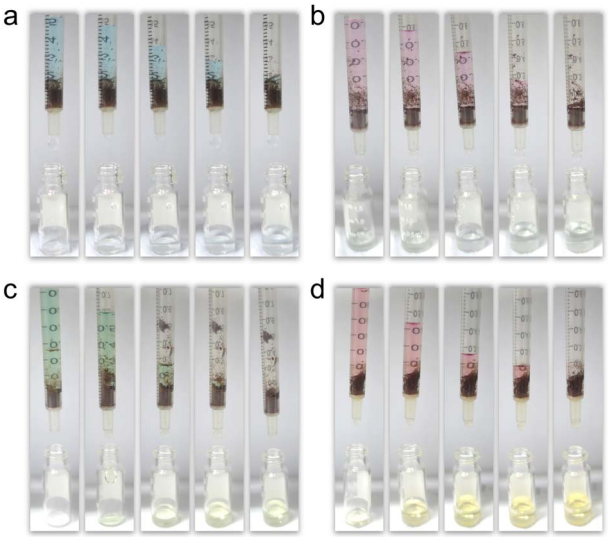

Fig. 5 Photographs of the **Ag46**-filled column-chromatographic separation process for (a) MB, (b) RhB, (c) MO/MB, and (d) MO/RhB.

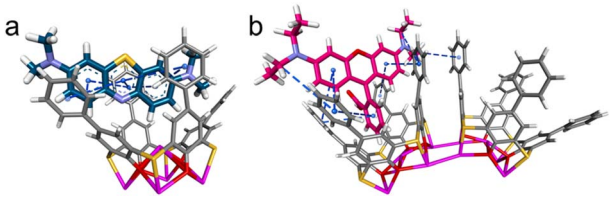

Fig. 6 Various interactions of **Ag46** with MB (a) or RhB (b). Colour code: Ag, purple; O, red; S, yellow; C, gray, sea blue, and dark pink; N, blue; H, white. The noncovalent interactions are shown with a dashed light blue line.

Conclusions

To summarize, we have presented a systematic strategy for the self-assembly of heteroanions that controls the shape and expansion of the silver nanowheels from Ag_{37} to Ag_{46} with the assistance of the macrocyclic $PTC4A^{4-}$ ligand. Structural determination revealed that when using chloride ions as a template, self-assembly resulted in the construction of **Ag37**, which indicated that chloride ions act as local and global anion templates and are crucial for the organization of a pentagonal silver shell. In contrast in **Ag46**, when chromate ions along with chloride ions were used as templates, the chromate ions served as the local template, and the chloride ions served as the global template to build a unique hexagonal silver shell. The chromate ions are bulkier and carry more negative charges, which increases their coordination ability with silver atoms, and it is believed to trigger the structural expansion of the silver core and silver shell. Interestingly, the hydrophobic cavity of the $PTC4A^{4-}$ ligand on the surface of **Ag46** selectively captures cationic dyes (MB and RhB) through host–guest interaction. Our present work expands the scope of controlled synthesis, expansion, and organization of high-nuclearity silver NCs regulated by

a heteroanion template and provides a feasible way of designing NC assemblies with various geometries and functional properties.

Data availability

All experimental procedures, characterization data, and experimental spectra that support the findings of this study are available in the main text and ESI.†

Author contributions

D. S. supervised the project; R. K. G. and L. L. performed the experiments; R. K. G., L. L., Z. W., B. L. H., L. F., Z. Y. G., C. H. T., and D. S. analyzed the data, prepared the figures, and provided conceptual contributions; R. K. G., L. L., and D. S. wrote the manuscript through contributions from all authors. All authors have given their approval to the final version of the manuscript.

Conflicts of interest

There are no conflicts to declare.

Acknowledgements

This work was financially supported by the National Natural Science Foundation of China (Grant No. 52261135637, 22201159, 22171164, 91961105, and 22150410333), the Natural Science Foundation of Shandong Province (No. ZR2022QB008, ZR2020ZD35 and ZR2019ZD45), the Taishan Scholar Project of Shandong Province of China (No. tsqn201812003 and ts20190908), the National Postdoctoral Innovative Talents Support Program (No. BX2021171) and China Postdoctoral Science Foundation (No. 2021M700081).

Notes and references

1 (*a*) J. P. Wilcoxon and B. L. Abrams, *Chem. Soc. Rev.*, 2006, **35**, 1162–1194; (*b*) S. Yamazoe, K. Koyasu and T. Tsukuda, *Acc. Chem. Res.*, 2014, **47**, 816–824; (*c*) Y. P. Xie, J. L. Jin, G. X. Duan, X. Lu and T. C. W. Mak, *Coord. Chem. Rev.*, 2017, **331**, 54–72; (*d*) R. C. Jin, C. J. Zeng, M. Zhou and Y. X. Chen, *Chem. Rev.*, 2016, **116**, 10346–10413; (*e*) J. F. Corrigan, O. Fuhr and D. Fenske, *Adv. Mater.*, 2009, **21**, 1867–1871; (*f*) A. Fernando, K. L. D. M. Weerawardene, N. V. Karimova and C. M. Aikens, *Chem. Rev.*, 2015, **115**, 6112–6216; (*g*) M. Ueda, Z. L. Goo, K. Minami, N. Yoshinari and T. Konno, *Angew. Chem., Int. Ed.*, 2019, **58**, 14673–14678.

2 (*a*) C. J. Zeng, Y. X. Chen, K. Kirschbaum, K. J. Lambright and R. C. Jin, *Science*, 2016, **354**, 1580–1584; (*b*) Y. Jin, C. Zhang, X. Y. Dong, S. Q. Zang and T. C. W. Mak, *Chem. Soc. Rev.*, 2021, **50**, 2297–2319; (*c*) C. J. Zeng, Y. X. Chen, K. Kirschbaum, K. Appavoo, M. Y. Sfeir and R. C. Jin, *Sci. Adv.*, 2015, **1**, e1500045; (*d*) Y. Y. Liu, B. K. Najafabadi, M. A. Fard and J. F. Corrigan, *Angew. Chem., Int. Ed.*, 2015, **54**, 4832–4835; (*e*) K. Yonesato, H. Ito, H. Itakura, D. Yokogawa, T. Kikuchi, N. Mizuno, K. Yamaguchi and K. Suzuki, *J. Am. Chem. Soc.*, 2019, **141**, 19550–19554.

3 (*a*) Q. M. Wang, Y. M. Lin and K. G. Liu, *Acc. Chem. Res.*, 2015, **48**, 1570–1579; (*b*) R. Ge, X. X. Li and S. T. Zheng, *Coord. Chem. Rev.*, 2021, **435**, 213787; (*c*) D. Rais, J. Yau, D. M. P. Mingos, R. Vilar, A. J. P. White and D. J. Williams, *Angew. Chem., Int. Ed.*, 2001, **40**, 3464–3467; (*d*) Z. Wang, R. K. Gupta, G. Luo and D. Sun, *Chem. Rec.*, 2020, **20**, 389–402.

4 (*a*) Z. H. Pan, C. L. Deng, Z. Wang, J. Q. Lin, G. G. Luo and Di Sun, *CrystEngComm*, 2020, **22**, 3736–3748; (*b*) Y. L. Shen, P. Zhao, J. L. Jin, J. Han, C. Liu, Z. Liu, M. Ehara, Y. P. Xie and X. Lu, *Dalton Trans.*, 2021, **50**, 10561–10566.

5 Y. P. Xie and T. C. W. Mak, *Angew. Chem., Int. Ed.*, 2012, **51**, 8783–8786.

6 J. W. Liu, H. F. Su, Z. Wang, Y. A. Li, Q. Q. Zhao, X. P. Wang, C. H. Tung, D. Sun and L. S. Zheng, *Chem. Commun.*, 2018, **54**, 4461–4464.

7 (*a*) J. Z. Yan, B. K. Teo and N. F. Zheng, *Acc. Chem. Res.*, 2018, **51**, 3084–3093; (*b*) J. Yang and R. C. Jin, *ACS Mater. Lett.*, 2019, **1**, 482–489; (*c*) Q. F. Yao, T. K. Chen, X. Yuan and J. P. Xie, *Acc. Chem. Res.*, 2018, **51**, 1338–1348.

8 (*a*) A. Desireddy, B. E. Conn, J. Guo, B. Yoon, R. N. Barnett, B. M. Monahan, K. Kirschbaum, W. P. Griffith, R. L. Whetten, U. Landman and T. P. Bigioni, *Nature*, 2013, **501**, 399–402; (*b*) H. Y. Yang, Y. Wang, H. Q. Huang, L. Gell, L. Lehtovaara, S. Malola, H. Hakkinen and N. F. Zheng, *Nat. Commun.*, 2013, **4**, 2422; (*c*) C. P. Joshi, M. S. Bootharaju, M. J. Alhilaly and O. M. Bakr, *J. Am. Chem. Soc.*, 2015, **137**, 11578–11581.

9 (*a*) G. X. Duan, J. Han, B. Z. Yang, Y. P. Xie and X. Lu, *Nanoscale*, 2020, **12**, 1617–1622; (*b*) M. Diecke, C. Schrenk and A. Schnepf, *Angew. Chem., Int. Ed.*, 2020, **59**, 14418–14422.

10 (*a*) M. M. Zhang, X. Y. Dong, Y. J. Wang, S. Q. Zang and T. C. W. Mak, *Coord. Chem. Rev.*, 2022, **453**, 214315; (*b*) M. Qu, H. Li, L. H. Xie, S. T. Yan, J. R. Li, J. H. Wang, C. Y. Wei, Y. W. Wu and X. M. Zhang, *J. Am. Chem. Soc.*, 2017, **139**, 12346–12349.

11 (*a*) W. J. Du, S. Jin, L. Xiong, M. Chen, J. Zhang, X. J. Zou, Y. Pei, S. X. Wang and M. Z. Zhu, *J. Am. Chem. Soc.*, 2017, **139**, 1618–1624; (*b*) H. Y. Yang, J. Z. Yan, Y. Wang, H. F. Su, L. Gell, X. J. Zhao, C. F. Xu, B. K. Teo, H. Hakkinen and N. F. Zheng, *J. Am. Chem. Soc.*, 2017, **139**, 31–34; (*c*) M. J. Alhilaly, M. S. Bootharaju, C. P. Joshi, T. M. Besong, A. H. Emwas, R. Juarez-Mosqueda, S. Kaappa, S. Malola, K. Adil, A. Shkurenko, H. Hakkinen, M. Eddaoudi and O. M. Bakr, *J. Am. Chem. Soc.*, 2016, **138**, 14727–14732; (*d*) Y. T. Chen, I. S. Krytchankou, A. J. Karttunen, E. V. Grachova, S. P. Tunik, P. T. Chou and I. O. Koshevoy, *Organometallics*, 2017, **36**, 480–489; (*e*) H. Shen, K. Kubo, S. Kume, L. M. Zhang and T. Mizuta, *Dalton Trans.*, 2017, **46**, 16199–16204.

12 Z. Wang, L. Li, L. Feng, Z. Y. Gao, C. H. Tung, L. S. Zheng and D. Sun, *Angew. Chem., Int. Ed.*, 2022, **61**, e202200823.

13 Z. J. Guan, R. L. He, S. F. Yuan, J. J. Li, F. Hu, C. Y. Liu and Q. M. Wang, *Angew. Chem., Int. Ed.*, 2022, **61**, e202116965.

14 Z. J. Guan, F. Hu, S. F. Yuan, Z. A. Nan, Y. M. Lin and Q. M. Wang, *Chem. Sci.*, 2019, **10**, 3360–3365.
15 Z. J. Guan, J. L. Zeng, Z. A. Nan, X. K. Wan, Y. M. Lin and Q. M. Wang, *Sci. Adv.*, 2016, **2**, e1600323.
16 Z. Wang, H. F. Su, L. P. Zhang, J. M. Dou, C. H. Tung, D. Sun and L. S. Zheng, *ACS Nano*, 2022, **16**, 4500–4507.
17 Z. Wang, H. F. Su, Y. W. Gong, Q. P. Qu, Y. F. Bi, C. H. Tung, D. Sun and L. S. Zheng, *Nat. Commun.*, 2020, **11**, 308.
18 Z. Wang, F. Alkan, C. M. Aikens, M. Kurmoo, Z. Y. Zhang, K. P. Song, C. H. Tung and D. Sun, *Angew. Chem., Int. Ed.*, 2022, **61**, e202206742.
19 (*a*) R. Kumar, Y. O. Lee, V. Bhalla, M. Kumar and J. S. Kim, *Chem. Soc. Rev.*, 2014, **43**, 4824–4870; (*b*) M. Zhao, J. Lv and D. S. Guo, *RSC Adv.*, 2017, **7**, 10021–10050; (*c*) N. Frank, A. Dallmann, B. Braun-Cula, C. Herwig and C. Limberg, *Angew. Chem., Int. Ed.*, 2020, **59**, 6735–6739.
20 (*a*) M. Rubio-Martinez, C. Avci-Camur, A. W. Thornton, I. Imaz, D. Maspochbc and M. R. Hill, *Chem. Soc. Rev.*, 2017, **46**, 3453–3480; (*b*) A. Chen, X. Kang, S. Jin, W. J. Du, S. X. Wang and M. Z. Zhu, *J. Phys. Chem. Lett.*, 2019, **10**, 6124–6128; (*c*) B. E. Conn, A. Desireddy, A. Atnagulov, S. Wickramasinghe, B. Bhattarai, B. Yoon, R. N. Barnett, Y. Abdollahian, Y. W. Kim, W. P. Griffith, S. R. J. Oliver, U. Landman and T. P. Bigioni, *J. Phys. Chem. C*, 2015, **119**, 11238–11249.
21 (*a*) T. K. Chen, Q. F. Yao, R. R. Nasaruddin and J. P. Xie, *Angew. Chem., Int. Ed.*, 2019, **58**, 11967–11977; (*b*) A. Nag, P. Chakraborty, G. Paramasivam, M. Bodiuzzaman, G. Natarajan and T. Pradeep, *J. Am. Chem. Soc.*, 2018, **140**, 13590–13593; (*c*) Y. Niihori, M. Matsuzaki, T. Pradeep and Y. Negishi, *J. Am. Chem. Soc.*, 2013, **135**, 4946–4949; (*d*) Y. Shichibu, M. Zhang, Y. Kamei and K. Konishi, *J. Am. Chem. Soc.*, 2014, **136**, 12892–12895.
22 (*a*) J. B. Baruah, *Coord. Chem. Rev.*, 2022, **470**, 214694; (*b*) M. Najafi, S. Abednatanzi, P. G. Derakhshandeh, F. Mollarasouli, S. Bahrani, E. S. Behbahani, P. V. D. Voort and M. Ghaedi, *Coord. Chem. Rev.*, 2022, **454**, 214332.
23 Y. B. Zhou, J. Lu, Y. Zhou and Y. D. Liu, *Environ. Pollut.*, 2019, **252**, 352–365.
24 (*a*) C. Z. Sun, T. P. Sheng, F. R. Dai and Z. N. Chen, *Cryst. Growth Des.*, 2019, **19**, 1144–1148; (*b*) A. J. Gosselin, C. A. Rowland and E. D. Bloch, *Chem. Rev.*, 2020, **120**, 8987–9014.
25 P. Lhotak, T. Smejkal, I. Stibor, J. Havlicek, M. Tkadlecova and H. Petrickova, *Tetrahedron Lett.*, 2003, **44**, 8093–8097.